1-1-2014

Case studies on response of laterally loaded nonlinear piles

Wei Dong Guo
University of Wollongong, wdguo@uow.edu.au

Case studies on response of laterally loaded nonlinear piles

Abstract

Closed-form solutions for laterally loaded free and fixed-head piles in elastic-plastic media have been developed and implemented into a spreadsheet program called GASLFP. Underpinned by a generic limiting force profile (LFP), the solutions offer an expeditious and sufficiently accurate method for predicting response of lateral piles. They also allow parameters to be deduced using measured pile response, as is evident in the study to date on -70 test (elastic) piles. The solutions also well capture the impact of structure nonlinearity of pile body by employing reduced pile bending stiffness (EpIp). The law of the reduction in EpIp, however, needs to be verified. In this paper, the solutions are utilised to examine the response of four test-piles exhibiting structural nonlinearity. For each nonlinear concrete pile, the shear modulus of soil and the three parameters (of Ng, ao and n) for constructing the LFP were deduced first using elastic pile assumption; and subsequently the variations of flexural rigidity with bending moment, the cracking moment Mcr and the ultimate moment Mult were back-figured against measured pile deflection. Thie study provides parameters for modelling nonlinear piles in sand and clay, and justification using pertinent expressions.

Keywords

case, laterally, studies, loaded, nonlinear, piles, response

Disciplines

Engineering | Science and Technology Studies

Publication Details

Guo, W. Dong. (2014). Case studies on response of laterally loaded nonlinear piles. Geotechnical Engineering, 45 (2), 70-77.

Case Studies on Response of Laterally Loaded Nonlinear Piles

Wei Dong Guo[1]
[1] *School of Civil, Environmental and Mining Engineering, University of Wollongong, Wollongong, Australia*
E-mail: wdguo@uow.edu.au

ABSTRACT: Closed-form solutions for laterally loaded free and fixed-head piles in elastic-plastic media have been developed and implemented into a spreadsheet program called GASLFP. Underpinned by a generic limiting force profile (LFP), the solutions offer an expeditious and sufficiently accurate method for predicting response of lateral piles. They also allow parameters to be deduced using measured pile response, as is evident in the study to date on ~70 test (elastic) piles. The solutions also well capture the impact of structure nonlinearity of pile body by employing reduced pile bending stiffness (E_pI_p). The law of the reduction in E_pI_p, however, needs to be verified. In this paper, the solutions are utilised to examine the response of four test-piles exhibiting structural nonlinearity. For each nonlinear concrete pile, the shear modulus of soil and the three parameters (of N_g, α_o and n) for constructing the LFP were deduced first using elastic pile assumption; and subsequently the variations of flexural rigidity with bending moment, the cracking moment M_{cr} and the ultimate moment M_{ult} were back-figured against measured pile deflection. The study provides parameters for modelling nonlinear piles in sand and clay, and justification on using pertinent expressions.

1. INTRODUCTION

A free-head pile is subjected to a lateral load P_t at an eccentricity e (thus a moment, $M_t = P_t e$) above ground level (GL), as schematically shown in Figure 1(a). The pile-head is free to rotate and translate with no constraint imposed at the pile head and along the effective pile length except for soil resistance. A number of approaches based on p-y concept were developed to capture the behavior of elastic pile (McClelland and Focht 1958). Guo (2001) proposed to model the pile-soil interaction at each depth x (below the GL) by a spring in series with a slider characterized by an idealized elastic-plastic p-y curve (p = net resistance per unit length, y = deflection along the pile axis) [see Figure 1(b)]. The spring has a subgrade modulus, k (i.e. the slope of the p-y curve), and the slider provides a limiting force per unit length p_u for the interaction [see Figure 1(c)]. The resistance p normally reaches the p_u from the GL and gradually extends to a depth called slip depth, x_p with increasing loading. Above the depth, the pile-soil interaction is in plastic state; whereas below the slip depth, it is in elastic state. The elastic zone of the pile is modelled by the independent springs, and a fictitious membrane (with a constant fictitious tension, N_p) to incorporate the coupled effect among springs (Guo and Lee 2001).The plastic zone is captured by the p_u, as the tension is negligible (N_p = 0) (i.e. an uncoupled load transfer model).

The subgrade modulus k and the fictitious tension, N_p are theoretically correlated with Young's modulus of an equivalent solid pile, E_p [=$E_pI_p/(\pi d^4/64)$] and shear modulus of soil, G_s, in which E_pI_p and d = flexural rigidity, and outside diameter of the pile, respectively (Guo and Lee 2001). The limiting force per unit length p_u is well captured by (Guo 2001) (later referred to as *Guo* LFP).

$$p_u = A_L(\alpha_o + x)^n \tag{1}$$

where p_u = limiting force per unit length [FL^{-1}]; $A_L = s_u N_g d^{1-n}$ (clay), and $\gamma_s' N_g d^{2-n}$ (sand), gradient of the LFP [FL^{-1-n}]; α_o = a constant to include the force at the GL [L]; x = depth below the GL [L]; n = a power to the sum of α_o and x; N_g = limiting force factor; S_u = undrained shear strength of cohesive soil [FL^{-2}]; and γ_s' = effective unit weight of the soil [FL^{-3}]. Guo (2006) shows (1) G_s = (0.25 ~ 0.62)N (MPa) ($\tilde{G}_s = 0.5N$ MPa, note the bar denotes average; and N = blow counts of SPT); and α_o = 0, n = 1.7 and N_g = (0.4~2.5)K_p^2 with respect to a uniform sand profile; in which $K_p = \tan^2(45^o + \phi_s/2)$; and ϕ_s = effective friction angle of the soil (2) G_s = (25 ~315)s_u ($\tilde{G}_s = 92.3 s_u$); and n = 0.7, α_o = 0.05~0.2 m ($\tilde{\alpha}_o$ = 0.11m), and N_g = 0.6~3.2($\tilde{N}_g$ = 1.6) for a uniform clay profile. And (3) Use of an average G_s over a depth of 10d, and the construction of an average LFP for a layered soil profile.

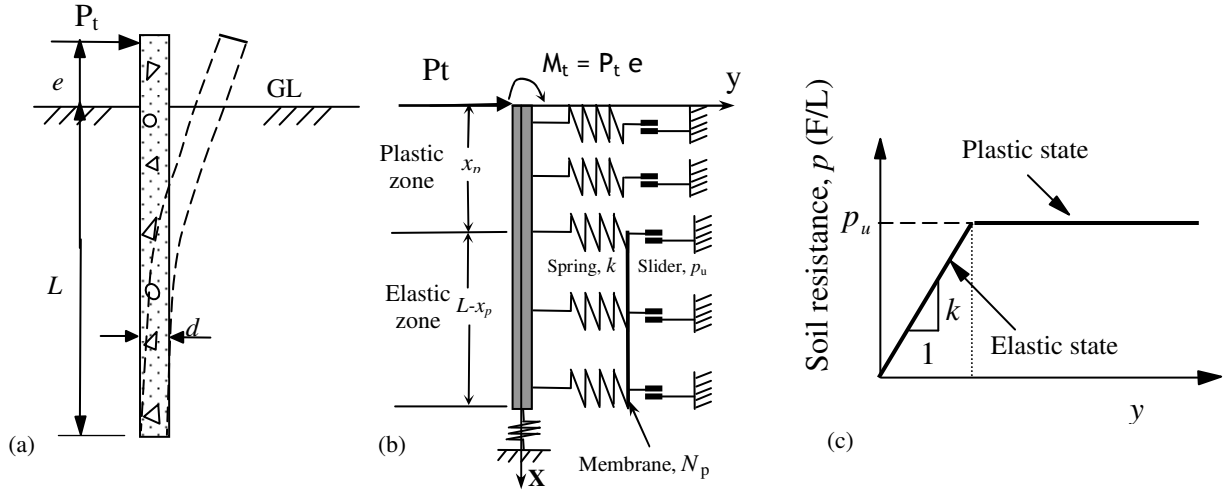

Figure 1 Coupled load transfer analysis for a free-head pile (Guo, 2001a, 2006): (a) The problem addressed, (b) Coupled load transfer model, and (c) Load transfer (p-y) curve

Other typical LFPs are defined previously (Guo 2006), such as Broms LFP (Broms 1964), Reese LFP for cohesionless soil (Reese et al. 1974), Matlock LFP for cohesive soil (Matlock 1970), and Hansen LFP for subsoil using cohesion c and ϕ_s' (Brinch Hansen 1961), which will be used directly herein.

In light of the 'Guo LFP', elastic-plastic, closed-form (CF) solutions were developed for laterally loaded piles (Guo 2006). They encompass explicit expressions for estimating pile deflection, slope, bending moment, shear force and soil resistance, as functions of reciprocal of characteristic length of the pile λ $\{= [k/(4E_pI_p)]^{0.25}\}$ with k/G_s= 2.4~3.92, the slip depth x_p and the parameters A_L (or N_g), α_o, and n (for the LFP). They are readily estimated using a spreadsheet program called GASLFP, and are provided in simple closed-form expressions for α_o= 0 and N_p = 0. For instance, ignoring ground level resistance (i.e. α_o = 0), and using a uncoupled model (N_p = 0), the pile deflection at GL y_o is given by

$$\frac{y_o k\lambda^n}{A_L} = \frac{2}{3}\bar{x}_p^{n+3}\frac{2\bar{x}_p^2+(2n+10)\bar{x}_p+n^2+9n+20}{(\bar{x}_p+1+\bar{e})(n+2)(n+4)} + \frac{(2\bar{x}_p^2+2\bar{x}_p+1)\bar{x}_p^n}{\bar{x}_p+1+\bar{e}} + \frac{4}{3}\bar{P}_t\bar{e}^3 + \frac{2\bar{x}_p^4+(n+4)(\bar{x}_p+1)[2\bar{x}_p^2+(n+1)(\bar{x}_p+1)]}{(\bar{x}_p+1+\bar{e})(n+1)(n+4)}\bar{e}\bar{x}_p^n \quad (2)$$

where $\bar{x}_p = \lambda x_p, \bar{e} = \lambda e$, and $\bar{P}_t = P_t\lambda^{1+n}/A_L$. The solutions and the program GASLFP well capture the nonlinear response of laterally loaded (elastic) piles.

Conversely, the program also allows the values of A_L (or N_g), α_o, *n, and* G_s to be deduced by matching the predicted with measured pile response, such as maximum bending moment (M_{max}), pile deflection y_o, and so forth under a spectrum of load P_t. The solutions are developed for a pile with a length $L > L_{cr}$ [$= 1.05d(E_p/G_s)^{0.25}$] in elastic zone; otherwise the solutions for short rigid piles (Guo 2008) should be adopted. Note the G_s may be taken as the average G_s over a depth of 10*d*. GASLFP is used to conduct current investigation. The solutions (and programs) also allow response of nonlinear piles to be captured through reducing pile bending stiffness after crack (normally seen in concrete piles at a large deflection), as outlined subsequently.

2. MODELLING STRUCTURE NONLINEARITY

Tensile crack may be developed at a large deflection of a laterally loaded concrete pile, once the tensile stress at the extreme fibre reaching the modulus of rupture f_r. Section analysis of a beam allows the modulus f_r to be correlated with cracking moment, M_{cr} (upon which cracks is initiated) by:

$$M_{cr} = f_r I_g / y_r = k_r\sqrt{f_c'}I_g / y_r \quad (3)$$

where k_r = 19.7~31.5 for a normal weight concrete beam (ACI. 1993), and 16.7~62.7 for lateral piles (revealed later); y_r = distance from centroidal axis of gross section to extreme fibres in tension; I_g = moment of inertia of gross section about centroidal axis neglecting reinforcement; f_c' = characteristic value of the compressive strength of concrete, in kPa. The f_c' and E_c may be empirically correlated by $E_c = 151{,}000(f_c')^{0.5}$ (kPa) (ACI. 1993), in absence of experimental data.

The crack occurs in a pile at the depth of M_{max} once $M_{max} > M_{cr}$, while other regions may still be intact. This will render reduction in the flexural rigidity of the pile from the elastic *EI* (= E_cI_g) to a new effective bending rigidity E_pI_p (= E_cI_e) until a final cracked rigidity $(EI)_{cr}$ (= E_cI_{cr}). Note I_{cr} = moment of inertia of cracked sections, at which fictitious hinges (thus ultimate bending moment, M_{ult}) takes place. The *EI* (or E_pI_p) represents the product of the modulus of elasticity of concrete, E_c and an effective moment of inertia, I_g (or I_e). The reduction in I_e with increase in M_{max} is currently based on the correlation proposed for beams (ACI. 1993), which may be written as

$$E_pI_p = \left(\frac{M_{cr}}{M_{\max}}\right)^3 EI + \left[1-\left(\frac{M_{cr}}{M_{\max}}\right)^3\right](EI)_{cr} \quad (4)$$

Equation (4) is used to deduce Young's modulus of a pile, E_p [= $E_cI_e/(\pi d^4/64)$, or $E_cI_e/(bh^3/12)$], for entire pile body, regardless of the position and scale of cracks. Replacing E_p in the elastic-pile solutions with this new E_p allows (structurally) nonlinear pile response to be captured using the same solutions for elastic piles (Guo 2006). The M_{max} may be gained using elastic-pile (*EI*) analysis (Guo and Zhu 2011) (but for piles with an extremely high EI), as it is only slightly affected by development of crack. The new E_pI_p for each M_{max} (or load) may be calculated using equation (4), together with M_{cr} from equation (3), and $(EI)_{cr}$ from **r**ectangular **b**lock **s**tress method (RBS) (Guo and Zhu 2011).

The solutions of elastic pile [e.g. equation (1)] well capture the impact of pile structure nonlinearity (Guo & Zhu 2011) via reducing the bending stiffness E_pI_p. The law of the reduction is examined herein against measured responses of structurally nonlinear piles (Nakai and Kishida 1982; Reese 1997; Huang et al. 2001; Ng et al. 2001; Zhang 2003) using GASLFP.

3. ANALYSIS OF FOUR NONLINEAR PILES

In this study, the M_{cr} (thus k_r) and E_pI_p are deduced using GASLFP and measured pile response, as are parameters G_s and LFP for linear piles. Six piles were studied with input and deduced parameters being summarized in Tables 1, 2 and 3. The measured M_{cr} defines the start of deviation between the predicted P_t–y_o curve using EI and the measured data. Thereafter, the E_pI_p is reduced to fit the predicted with the measured P_t- y_o curve until the final cracked rigidity $(EI)_{cr}$. The back-figured k_r is used to validate equation (3). The deduced values of E_pI_p at various levels of M_{max} along with M_{cr} and $(EI)_{cr}$ are adopted to justify equation (4) .

3.1 Case SN1 in Fine Sand

A bored pile B7 (termed as Case SN1) was instrumented with strain gauges and inclinometers, and tested under a lateral load applied near the GL (e = 0) (Huang et al. 2001). The soil profile at the site consisted of fine sand (SM) or silt (ML), and occasional silty clay. The ground water is located 1 m below the GL. The soil (to a depth of 15 m below the GL) had an average SPT blow count, $\tilde{N}$ of 16.9, a friction angle ϕ_s of 32.6º, and an effective unit weight, γ_s' of 10 kN/m^3. Thereafter, the SPT gradually increases from 25 (at a depth of 15 m) to 75 (at 80 m). The pile was 34.9 m in length, 1.5 m in diameter, and reinforced with 52 rebars (each had d = 32 mm and a yield strength f_y of 471 MPa). It had a concrete cover *t* of 50 mm thick with a compressive strength f_c' of 27.5 MPa. The *EI* and I_g were estimated as 6.86GN-m^2, and 0.2485 m^4 respectively, and thus E_p = 27.6 GPa. The cracking moment M_{cr} was estimated as 1.08~1.73 MN-m using equation (3), k_r = 19.7~31.5 and $y_r = d/2$ = 0.75 m. A ultimate moment M_{ult} of 8.77 MN-m, and $(EI)_{cr}$ of 1.021GN-m^2 [i.e. $(EI)_{cr}/EI$ = 0.149] were estimated using the RSB method.

Assuming an elastic pile, the response (with EI) was predicted using: (1) n = 1.7, α_o = 0 and N_g =10.02 (= $0.9K_p^2$), deduced from the DMT tests (Huang et al., 2001), which gives the Guo LFP in Figure 2(a); and (2) G_s = 10.8 MPa (= 0.64N) (Guo 2006). The

predicted load P_t – deflection y_o curve (denoted by EI) is shown in Figure 2(b), along with measured data, which indicates a cracking load P_t of 1.25 MN; and an ultimate capacity of 2.943 MN (indicating by fast increase in deflection). Thereby it follows: (1) A measured moment M_{cr} of 3.45 MN-m (at 1.25 MN) and k_r = 62.7 (i.e. 2~3 times that suggested by ACI). And (2) A measured M_{ult} of 10.5 MN-m (at 2943 kN). The E_pI_p deduced by fitting the measured P_t-y_o curve gives $(EI)_{cr}/EI$ = 0.55, and $(EI)_{cr}$ = 3.773GN-m^2. The deduced values of M_{ult} and $(EI)_{cr}$ are 1.2 and 3.7 times those estimated using RSB method, respectively.

Table 1 Summary of information about piles investigated

Case	Reference	Pile details						
		d (m)	L (m)	EI (GN-m^2)	e (m)	f'_c (MPa)	f_y (MPa)	t (mm)
SN1	Huang et al. (2001)	1.5	34.9	6.86	0	27.5	471	50
SN2[c]	Huang et al. (2001)	0.8	34.0	0.79	0	78.5 (20.6)[a]	1226 (471)	30
SN3	Ng et al. (2001)	1.5	28	10	0.75	49	460	
SN4 [b]	Zhang (2003)	0.86	51.1	47.67	0	43.4	460	75
CN1[c]	Nakai & Kishida (1977)	1.548	30	16.68	0.5	153.7		
CN2		1.2	9.5	2.54	0.35	27.5		

[a]: 78.5 is for the outer prestressed pipe pile and 20.6 for the infill;
[b]: 0.86×2.8 (m^2) for a rectangular pile; [c]: Guo and Zhu (2012)

Table 2 Nonlinear properties of piles investigated

Cases	References	M_{cr} from ACI mtd (MN-m) (1)	M_{cr} dedued (MN-m) (2)	k_r derived from (2)	M_{ult} (MN-m)	$(EI)_{cr}/EI$ (%)	L_c/d
SN1	Huang et al. (2001)	1.08~1.73	3.45	62.7	8.77	14.8	8.9
SN2[a]	Huang et al. (2001)	0.28~0.44	0.465	33.0	1.89	14.6	9.8
SN3	Ng et al. (2001)	1.44~ 2.31	3.34	45.5	4.0	40	9.9
SN4	Zhang (2003)	4.61~ 7.38	7.42	31.7	10.13	1.9	27.7
CN1[a]	Nakai & Kishida	2.81~ 4.50	2.38	16.7		30	13.3
CN2	(1977)	0.55~ 0.89	0.63	22.3		18	7.1

[a]: Guo and Zhu (2012)

Table 3 Sand properties and derived parameters for piles in sand

Case	Soil type	Soil properties				Input parameters		
		γ_s' (kN/m^3)	ϕ_s (°)	N	D_r (%)	N_g/K_p^2	G/N(MPa)	n
SN1	Submerged silty sand	10	32.6	16.9		0.9	0.64	
SN2 [a]	Submerged silty sand	10	32.6	16.9		1.0	0.64	$\alpha_0 = 0$
SN3	Submerged sand	11.9	35.3	17.1	44	1.2	0.64	n = 1.7
SN4	Silty sand with occasional gravel	13.3	49	32.5	61	0.55	0.4	

[a]: Guo and Zhu (2012)

Using the calculated $(EI)_{cr}$ of 1.021GN-m^2 (RSB method), M_{cr} = 3.45 MN-m, and M_{ult} = 10.5 MN-m, the E_pI_p was determined using equation (4) for each M_{max} (obtained using EI) and the resulted $(EI)_{cr}/EI$ versus M_{max} is plotted in Figure 3(a). This E_pI_p allows y_o, M_{max} and x_p, to be predicted for each specified load. The predicted P_t– y_o curve is plotted in Figure 2(b) (triangular dots), and the M_{max} in Figure 2(c). A comparison between the predictions using elastic EI and nonlinear E_pI_p indicates that: (1) The M_{max} predicted using E_pI_p is ~ 3.2% less than that gained using EI; and (2) The slip depth x_p at P_t = 2571 kN increases to 3.08d (using E_pI_p) from 2.49d (using EI); and the deflection y_o exceeds the measured by 115% [indicating the impact of using an accurate $(EI)_{cr}$].

The large difference between the back-estimated and the calculated values of $(EI)_{cr}$ implies a partial development of crack in this particular pile.

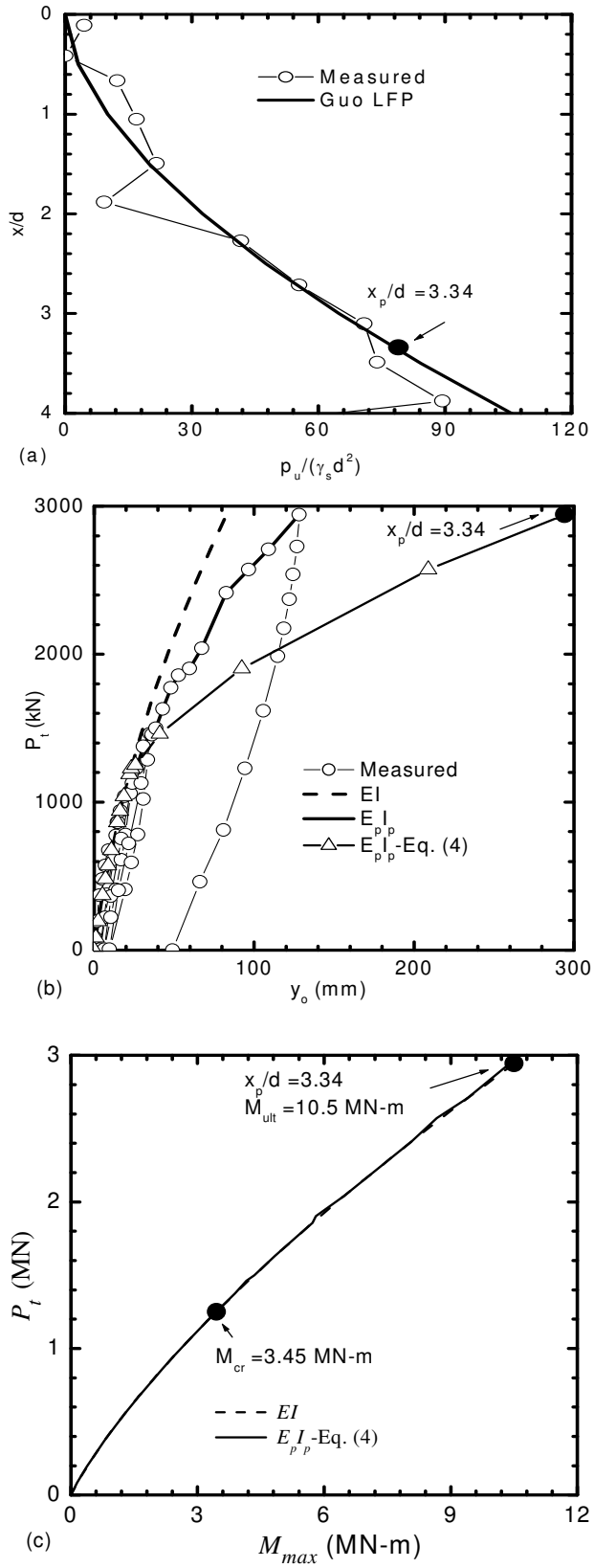

Figure 2 Comparison between measured (Huang et al., 2001) and predicted response of Pile B7: (a) LFPs, (b) P_t-y_o curves, and (c) P_t~M_{max} curves

3.2 Cases SN3 and SN4 in fill & Clay/Sand

3.2.1 Case SN3

Lateral loading test was conducted on a bored single pile embedded in very soft fill, followed by sandy estuarine deposit and clayey alluvium in Hong Kong (Ng et al. 2001). The ground water was located at 1.0 m below the GL. The sandy soil extending into a depth of 15m had $\tilde{N}$ = 17.1, ϕ_s = 35.3° (Guo and Zhu 2011), and γ_s' = 11.0 kN/m^3. Lateral loads were applied at the middle of the 1.5 m (thickness) pile-cap. The pile, 28 m long and 1.5 m in diameter, had the properties of f_y = 460 MPa, f_c' = 49 MPa, E_c = 32.3 GPa, EI =10 GN-m^2, $(EI)_{cr}$ = 4 GN-m^2, I_g = 0.2485 m^4, and E_p = 40.2 GPa. The M_{cr} was estimated as 1.44~2.31 MN-m using k_r = 19.7~31.5, y_r = 0.75 m and equation (3). The M_{ult} was not estimated owing to lack of the reinforcement detail.

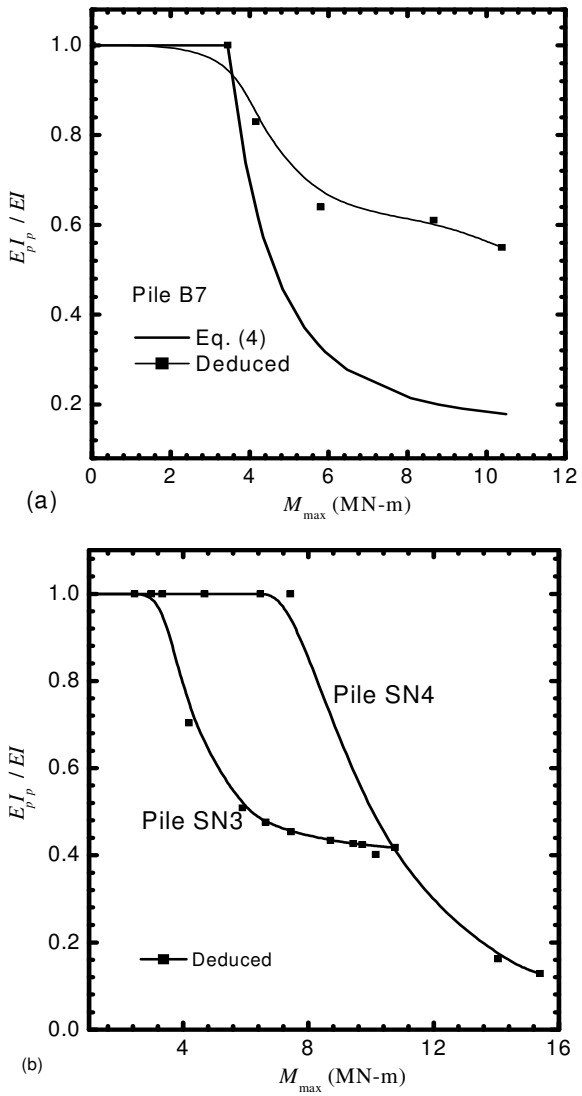

Figure 3 Variation of E_pI_p/EI ~ M_{max}.

The elastic pile analysis utilised $N_g = 1.2K_p^2$ = 16.76, α_o= 0 and n = 1.7 [see Figure 4(a)], and G_s = 10.9 MPa (= 0.64N). Note to a maximum slip depth x_p of 2.1d, the p_u value, as shown in Figure 4(a), exceeds the predictions of Broms' LFP and Reese's LFP. The predicted deflection y_o, as shown in Figure 4(b) by 'EI', agrees with the measured data up to P_t of 1.1 MN, at which M_{max} = 3.34 MN-m. This value, taking as measured M_{cr}, offers k_r = 45.5, which again is about twice that of the ACI's suggestion. The E_pI_p was deduced using the measured $P_t - y_o$ data, and is denoted as 'E_pI_p' in Figure 4(b). The associated P_t~M_{max} and E_pI_p/EI~M_{max} curves are plotted in Figures 4(c), and 3(b), respectively. In particular, it is noted that $(EI)_{cr}/EI$ = 0.4, and at a load of 2.955 MN, M_{max} = 10.77 MN-m and x_p = 2.1d. Equation (4) was not checked without the M_{ult}.

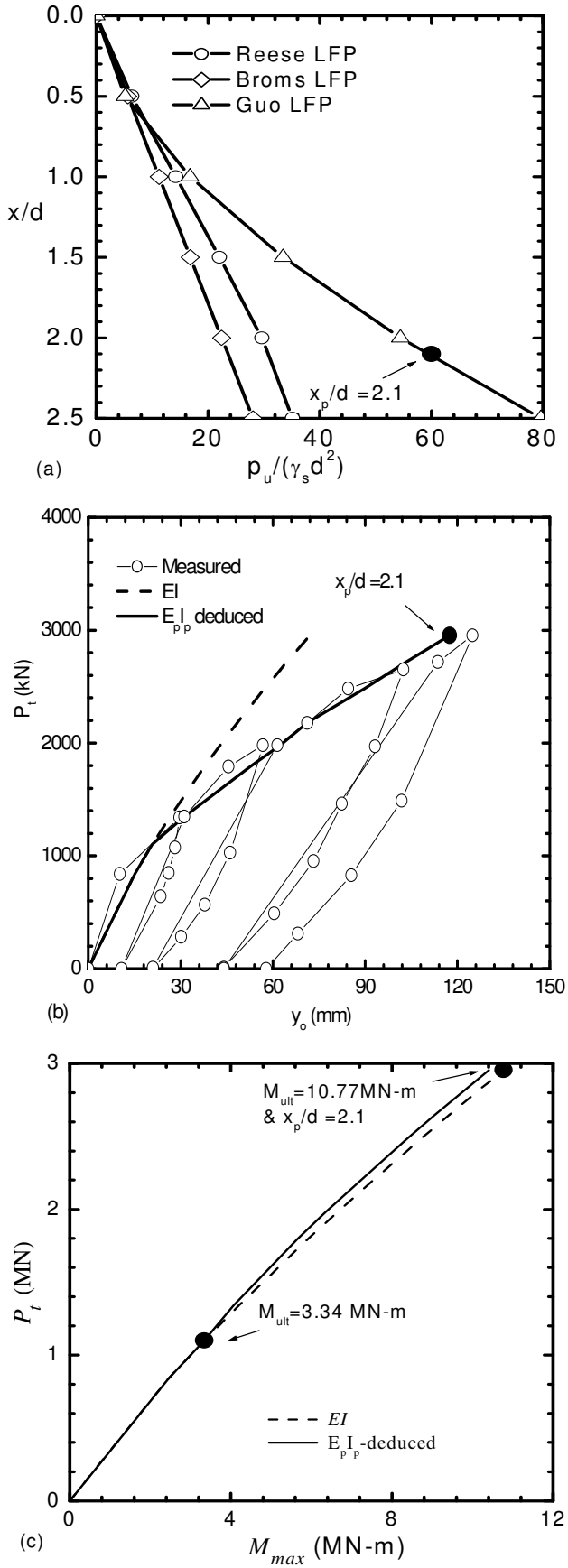

Figure 4 Comparison between measured (Ng, et al. 2001) and predicted response of Hong Kong pile: (a) LFPs, (b) P_t-y_o curves, and (c) P_t~M_{max} curves.

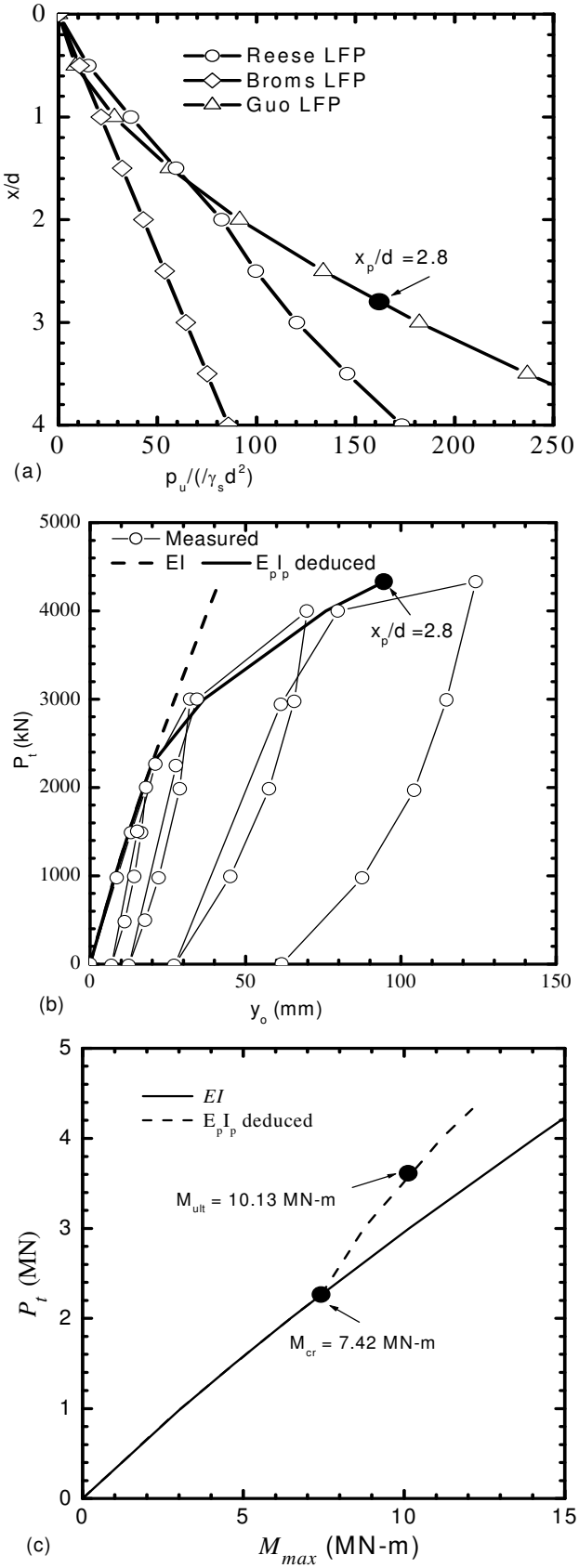

Figure 5 Comparison between measured (Zhang, 2003) and predicted response of DB1 pile: (a) LFPs, (b) P_t-y_o curves, and (c) P_t~M_{max} curve.

3.2.2 Case SN4

Lateral load tests were conducted on two big barrettes (DB1 and DB2) embedded to a depth of 20 m in a reclaimed land in Hong

Kong (Zhang 2003). The subsoil consisted either of sandy silty clay or loose to medium dense sand, and with cobbles in between the depths of 10.6~18.9 m below the GL. The ground water was located at a depth of 2.5 m. The soil properties (to a depth of 15 m) were $\overline{N}$ = 32.5, $\phi_s = 49^o$, and γ'_s = 13.3 kN/m^3. The barrette DB1 (called SN4 herein) was investigated, which had a length of 51.1 m, and a rectangular cross-section of 2.8 m (*height*) × 0.86 m. Load was applied along the height direction at near the GL (e = 0). The strength and stiffness properties were f_y = 460 MPa, f'_c = 43.4 MPa [= f_{cu}/1.22 (Beckett and Alexandrou 1997), and a cubic concrete compressive strength f_{cu} of 53 MPa], E_c = 30.3 GPa, t = 75-100 mm, I_g = 1.5732 m^4, *EI* = 47.67 GN-m^2, and $E_p = 1.78\times10^9$ kN-m^2. The M_{cr} was estimated as 4.61~7.38 MN-m using k_r = 19.7~31.5, and y_r = 1.4 m; and M_{ult} as 10.13 MN-m and $(EI)_{cr}$ as 0.89 GN-m^2 for the upper 15 m, using the RSB method.

The elastic-pile analysis adopts N_g = 28.15 (= $0.55K_p^2$), α_0 = 0, n = 1.7, and G_s = 13.0 MPa (= 0.4N). In particular, as shown in Figure 5(a), up to a depth of 1.5*d,* the current LFP lies in between Reese's LFP and Broms' LFP; and its average over a depth of ~2.8d is close to that from Reese's LFP. The predicted deflection y_o, see Figure 5(b), agrees well with the measured data until the cracking load of 2.26 MN, which gives a measured M_{cr} of 7.42 MN-m and k_r of 31.7. Using the M_{cr}, and $(EI)_{cr}$ of 0.89 GN-m^2, the E_pI_p, as shown in Figure 3(b), was deduced by matching the predicted and the measured deflection y_o [see Figure 5(b)], with the associated P_t~M_{max} curve being depicted in Figure 5(c). These figures indicate*:* (1) the M_{ult} of 10.13 MN-m occurs at $P_t \approx 3.61MN$, with the measured y_o increasing sharply; (2) The initiation of crack renders increase of (i) the x_p at the maximum load P_t of 4.33 MN by 27.8%; and (ii) the M_{max} by 26.9%. The increase in M_{max} is not generally expected for piles with a normal relative stiffness E_p/G^*, but for the excessively high E_p/G^* of 1.1×10^5 [G^* =(1+0.75ν_s)G_s, ν_s = Poisson's ratio]. It is not difficult to use the increased M_{max} from nonlinear analysis in equation (4).

3.3 Pile Test (Case CN2) in Clay

Test Pile *E* was conducted at a clay site with SPT values (depth) of N= 0 (0~2 m), and N = 4 ~ 6(2 ~10 m), and S_u =163.5 kPa at x = 3 m below the GL. Lateral load was applied 0.35 m above the GL. The pile was characterised by L = 9.5 m, d = 1.2 m, EI = 2.54 GN-m^2, and $f'_c \approx 27.5$ MPa [= $(E_c/151000)^2$]. The reported *EI* of 115.28 MN-m^2 (Nakai & Kishida 1982) was too low, as it gives an E_p of 1.13 GPa. Taking E_c (E_p) as the concrete modulus of 25 GPa, the M_{cr} was estimated as 554.2 ~ 886.7 kN-m (using k_r = 19.7~31.5, and y_r = 0.6 m). This value is slightly higher than 527.6 kN-m by Nakai & Kishida (1977), implying the rationale of the E_c. The M_{ult} is not determined without the reinforcement detail. The model of elastic-pile utilises n = 0.7, N_g = 2, α_o = 0.06 [see Figure 6(a)], G_s = 21.38 MPa (= 130.8S_u) (Nakai and Kishida 1982), and k = 3.77G_s. Up to a depth of 5*d*, Guo LFP is close to Hansen's LFP using c = 8 kPa and ϕ_s = 10°, but it is less than Matlock's LFP. The predicted pile deflection agrees well with the observed data up to P_t of 470 kN [see Figure 6(b)]. The measured M_{cr} (M_{max} at P_{cr} = 470 kN) was computed as 628.4 kN-m and k_r as 22.3. The E_pI_p was deduced using the measured deflection y_o [see Figure 6(b)]. This in particular, offers E_pI_p/EI = 0.6 and 0.18, respectively, for P_t = 588.6 kN and 735.8 kN, which in turn offer $(EI)_{cr}/EI$ of 0.35 and 0.005, respectively, as per equation (4). The drastic drop in $(EI)_{cr}$ implies pile failure prior to 735.8 kN (Nakai and Kishida 1982). The predicted bending moment profiles basically agree with the scattered, measured data as shown in Figure 6(c), in light of the difficulty in obtaining reliable measured profiles after crack.

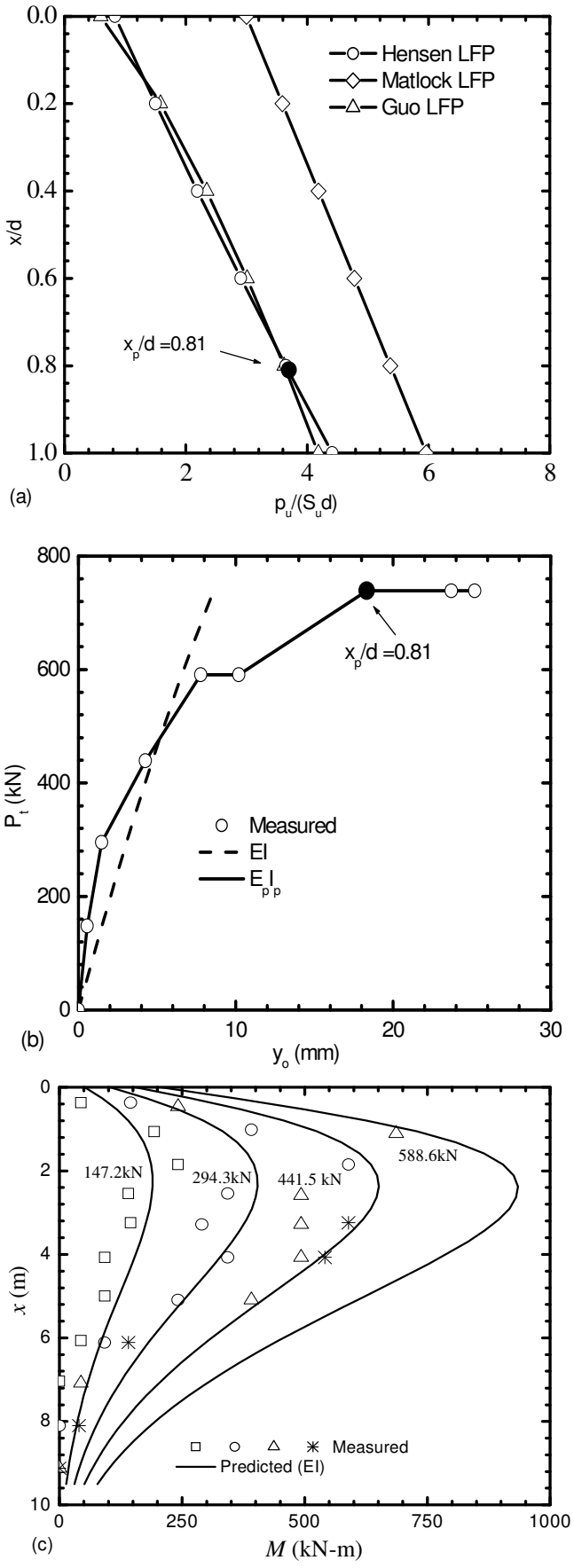

Figure 6 Comparison between calculated and measured (Nakai & Kishida, 1982) response of Pile E: (a) LFPs, (b) P_t-y_o curves, and (c) M profiles for P_t = 147.2 kN, 294.3 kN, 441.5 kN, and 588.6kN

The deduced variations of the normalised critical bending stiffness E_pI_p/EI with normalised bending moment M_{cr}/M_{max} for typical piles are plotted in Figure 7(a) together with those from three rock-socket piles (Guo 2012). The figure indicates a good agreement between each group of deduced dots and Equation (4) using the corresponding ratios of $(EI)_{cr}/EI$ (deduced). It is also interesting to see a linear correlation between the deduced values of k_r and $(EI)_{cr}/EI$ for all cases [see Figure 7(b)].

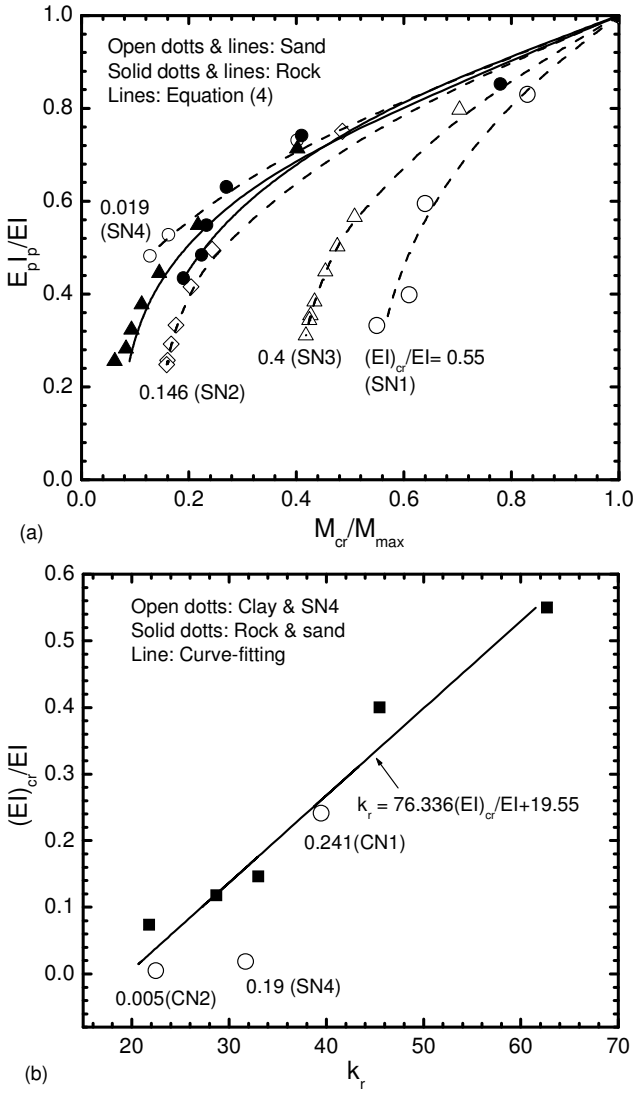

Figure 7 Normalised $(EI)_{cr}/EI$ versus (a) Normalised moment M_{cr}/M_{max}, and (b) the factor k_r

4. CONCLUSION

Study on six laterally loaded (structurally nonlinear) piles to date indicates similar ranges of soil parameters to elastic piles in clay, sand or layered soil, respectively, and the following features:

- The ultimate bending moment M_{ult}, flexural rigidity of cracked cross section E_pI_p may generally be evaluated using the method recommended by ACI (1993) [thus equation (4)], although this would not always offer good prediction of measured pile response such as cases SN1 and SN4.
- Using equation (3) to predict the cracking moment, the k_r should be taken as 16.7~22.3 (clay) and 31.7~62.7(sand). The k_r for piles in sand/ rock may be 2~ 3 times that for piles in clay and structural beams, and is linearly dependent of $(EI)_{cr}/EI$.

The current approach is underpinned by a reduced bending stiffness for entire piles. It well captures the overall response of a crack pile, but its accuracy to predicting profiles of bending moment and deflection is yet to be confirmed by reliable measured data to be gained.

Dr. Bitang Zhu assisted the preliminary calculation.

5. REFERENCES

ACI. (1993). Bridges, substructures, sanitary, and other special structures-structural properties. American Concrete Institute (ACI) Manual of Concrete Practice 1993, Part 4. Detroit.

Beckett, D. and A. Alexandrou (1997). Introduction to Eurocode 2: design of concrete structures (including seismic actions). London, Spon Press.

Brinch Hansen, J. (1961). The ultimate resistance of rigid piles against transveral forces. Copenhagen, Denmark, The Danish Geotechnical Institute Bulletin No. 12.

Broms, B. B. (1964). "Lateral resistance of piles in cohesionless soils." Journal of Soil Mechanics and Foundation Engineering Division, American Society of Civil Engineers, Vol. 90**,** No.3: pp.123-156.

Guo, W. D. (2001). Lateral pile response due to interface yielding. Proceedings of 8th International Conference Civil and Structural Engineering Computing, CIVIL-COMP2001, paper 108, Eisenstadt, nr Vienna, Austria.

Guo, W. D. (2006). "On limiting force profile, slip depth and lateral pile response." Computers and Geotechnics, Vol. 33**,** No.1: pp.47-67.

Guo, W. D. (2008). "Laterally loaded rigid piles in cohesionless soil." Canadian Geotechnical Journal, Vol. 45**,** No.5: pp.676-697.

Guo, W. D. (2012). Theory and Practice of Pile Foundations. London, Florida, CRC press.

Guo, W. D. and F. H. Lee (2001). "Load transfer approach for laterally loaded piles." International Journal for Numerical and Analytical Methods in Geomechanics, Vol. 25**,** No.11: pp.1101-1129.

Guo, W. D. and B. T. Zhu (2011). "Structure nonlinearity and response of laterally loaded piles." Australian Geomechanics, Vol. 46**,** No.3: pp.41-52.

Huang, A. B., C. K. Hsueh, M. W. O'Neill, S. Chern and C. Chen (2001). "Effects of construction on laterally loaded pile groups." Journal of Geotechnical and Geoenvironmental Engineering Division, ASCE, Vol. 127**,** No.5: pp.385-397.

Matlock, H. (1970). Correlations for design of laterally loaded piles in soft clay. Proceedings of the 2nd offshore technology conference, Houston, Texas, 577-594

McClelland, B. and J. A. Focht (1958). "Soil modulus for laterally loaded piles." Transactions, American Society of Civil Engineers, No.Paper No. 2954: pp.1049-1063.

Nakai, S. and H. Kishida (1982). Nonlinear analysis of a laterally loaded pile. Proceedings 4th International Conference on Numerical Methods in Geomechanics, Edmonton, 835-842.

Ng, C. W. W., L. Zhang and D. C. N. Nip (2001). "Response of laterally loaded large-diameter bored pile groups." Journal of Geotechnical and Geoenvironmental Engineering Division, ASCE, Vol. 127**,** No.8: pp.658-669.

Reese, L. C. (1997). "Analysis of laterally loaded shafts in weak rock." Journal of Geotechnical and Geoenvironmental Engineering Division, ASCE, Vol. 123**,** No.11: pp.1010-1017.

Reese, L. C., W. R. Cox and F. D. Koop (1974). Analysis of laterally loaded piles in sand. Proceedings 6th Annual Offshore Technology Conference, OTC. 2080, Dallas, Texas, 473-483.

Zhang, L. M. (2003). "Behavior of laterally loaded large-section barrettes." Journal of Geotechnical and Geoenvironmental Engineering Division, ASCE, Vol. 129**,** No.7: pp.639-648.

6. APPENDIX I. – Notation

The following symbols have been adopted in this paper.

A_L gradient of the LFP [FL^{-1-n}];
b width of a rectangular cross section of a pile;
d pile diameter;
e eccentricity of loading above groundline (GL);
E_c modulus of elasticity of concrete;
E_cI_g initial flexural rigidity of the pile;
E_p equivalent Young's modulus of pile;
f_c' characteristic value of compressive strength of the concrete;
f_c'' design value of concrete compressive strength;
f_y yield strength of reinforcement;
G_s shear modulus of soil;
h depth of a rectangular cross section of a pile;
I_g moment of inertia of gross section of the pile;
I_e effective moment of inertia of the pile after cracking;
I_{cr} moment of inertia of cracked section;
k subgrade modulus of a spring between pile and soil;
k_r a constant for concrete rupture;
L_{cr} critical length of a pile;
M_{cr} cracking moment;
M (M_{max}) bending moment in the pile (maximum M);
M_t moment applied at the pile at the GL;
n power to the sum of α_0 and x;
N blow count of Standard Penetration Tests (SPT) test;
N_g a gradient correlated compressive strength with the limiting pile – soil pressure at ground level;
N_p fictitious tension of a fictitious membrane linking the springs around the pile;
P_t lateral load applied at pile head;
p_u limiting force per unit length [FL^{-1}];
r pile radius;
s_u undrained shear strength [FL^{-2}];
x depth below ground level [L];
x_p slip depth;
y (y_o) pile deflection (y at ground level);
α_o a constant to include the force at ground level [L];
ϕ_s angle of friction of soil;
γ load transfer factor;
γ_s (γ_s') unit weight of the soil (effective γ_s);
θ the curvature.
λ reciprocal of characteristic length of the pile;
ν_s Poisson's ratio of soil;